JMEPEG (2018) 27:2381–2387
https://doi.org/10.1007/s11665-018-3314-x

1059-9495/$19.00

Effect of Sputtering Current on the Comprehensive Properties of (Ti,Al)N Coating and High-Speed Steel Substrate

Yongyao Su, Liangliang Tian, Rong Hu, Hongdong Liu, Tong Feng, and Jinbiao Wang

(Submitted March 22, 2017; in revised form January 26, 2018; published online March 30, 2018)

To improve the practical property of (Ti,Al)N coating on a high-speed steel (HSS) substrate, a series of sputtering currents were used to obtain several (Ti,Al)N coatings using a magnetron sputtering equipment. The phase structure, morphology, and components of (Ti,Al)N coatings were characterized by x-ray diffraction, scanning electron microscopy, energy-dispersive x-ray spectroscopy, and x-ray photoelectron spectroscopy, respectively. The performance of (Ti,Al)N coatings, adhesion, hardness, and wear resistance was tested using a scratch tester, micro/nanohardness tester, and tribometer, respectively. Based on the structure–property relationships of (Ti,Al)N coatings, the results show that both the Al content and deposition temperature of (Ti,Al)N coatings increased with sputtering current. A high Al content helped to improve the performance of (Ti,Al)N coatings. However, the HSS substrate was softened during the high sputtering current treatment. Therefore, the optimum sputtering current was determined as 2.5 A that effectively increased the hardness and wear resistance of (Ti,Al)N coating.

Keywords high-speed steel, property, sputtering current, structure, (Ti,Al)N coating

1. Introduction

High-speed steel (HSS) has excellent hardness, wear resistance, and heat resistance. Therefore, HSS is widely used in metal cutting and forming fields such as drills, taps, milling cutters, and broaches (Ref 1, 2). However, in some special practical situations such as the cutting of a hardened steel using a gear hobbing cutter, the hardness and wear resistance of HSS cannot satisfy the requirements. To solve this problem, coatings with higher hardness and wear resistance should be deposited on an HSS substrate. Titanium nitride (TiN) coating is one such coating to improve the performance of HSS owing to its high hardness and wear resistance and excellent chemical stability (Ref 3, 4).

Recently, better performance (thermal stability, wear resistance, etc.) of TiN coatings was achieved by adding aluminum (Al), chromium (Cr), molybdenum (Mo), vanadium (V), and yttrium (Y) by magnetron sputtering (Ref 5-12). For example, enhanced oxidation resistance (~ 850 °C) and higher hardness (~ 33, GPa) were achieved by adding Al. Al atoms replace the Ti atoms in a face-centered cubic structure and change the microstructure, leading to improved physical, chemical, and mechanical properties (Ref 13-15). The applications of (Ti,Al)N coatings in the tool coating field have been widely studied. However, most studies focused on the effect of Al on the properties of (Ti,Al)N coatings, but ignored the effect of substrate (Ref 16-18). The performance of (Ti,Al)N coatings strongly depends on the mechanical properties of substrate (Ref 19). According to our previous study (Ref 20), the hardness of an HSS substrate decreased at a high temperature, resulting in poor adhesion between the coating and substrate. Thus, it is of great importance to study the overall performance of a coating–substrate system instead of the coatings.

In our previous study (Ref 20), we studied only the effect of trace Al content on the structure and properties of a TiN coating. The result showed that trace Al did not change the microscopic structure of the TiN coating, but improved the hardness and wear resistance of the TiN coating. In this study, we investigated the effect of a high Al content on the structure and properties of TiN coating; we further studied the properties of coating–substrate system to improve the life of (Ti,Al)N-coated HSS tools. Moreover, different process parameters including sputtering current and deposition temperature were considered to evaluate their effect on the structure and properties of (Ti,Al)N coating. For this purpose, four (Ti,Al)N coatings were fabricated on HSS substrates using a medium-frequency reactive magnetron sputtering equipment at various sputtering currents. The composition, phase structure, coating–substrate adhesion, hardness, and wear of the (Ti,Al)N coatings were characterized. The tribological properties were evaluated using a tribometer. In addition, the effects of Al content and deposition temperature on the mechanical properties, chemical composition, and wear properties of the (Ti,Al)N coatings were evaluated. This study helps to better understand the relationship between sputtering current and performance of a coating–substrate system.

2. Experimental

2.1 Preparation of Sample and Process Conditions

The substrate was a M2 HSS with a size of Φ 20 × 3 mm. The substrate was mechanically ground, polished, and ultrasonically

Yongyao Su and Liangliang Tian contributed equally to this work.

Yongyao Su, Liangliang Tian, Rong Hu, Hongdong Liu, Tong Feng, and **Jinbiao Wang**, Research Institute for New Materials Technology, Chongqing University of Arts and Sciences, Chongqing 402160, People's Republic of China. Contact e-mails: hurong_82@163.com and wjbdys7983@163.com.

cleaned with acetone and ethanol. Then, the surface of the sample was cleaned by argon plasma sputtering. After the argon plasma sputtering, a 50 nm of Ti interlayer was deposited on the HSS substrate by ion-plating evaporation. Then, N_2 was introduced into the chamber to produce a TiN coating. A (Ti,Al)N coating was directly simultaneously deposited on the TiN interlayer by ion-plating Ti evaporation and sputtering TiAl (atomic ratio, 50:50) alloy with a size of 240 mm × 100 mm × 10 mm purchased from Antai Technology (China). Herein, the chemical composition of the (Ti,Al)N coatings was adjusted by varying the sputtering current (0, 1.5, 2.5, and 5 A), and they were named as $(Ti,Al)_{0A}N$, $(Ti,Al)_{1.5A}N$, $(Ti,Al)_{2.5A}N$, and $(Ti,Al)_{5A}N$, respectively. To evaluate the deposition temperature, a thermocouple thermometer with a display system was fixed on the vacuum chamber wall near the treated sample, providing a reference temperature. The other details about experimental parameters are shown in Table 1. The preparation system of coating was combined with medium-frequency reactive magnetron sputtering and ion-plating evaporation (Institute of industrial technology, Sichuan University, China). Ion-plating evaporation was used to enhance the ionization in the chamber and deposition of TiN coating. The medium-frequency reactive magnetron sputtering was used to introduce Al, Ti, Si elements. Compared with conventional magnetron sputtering, this coating system shows a higher ionization rate.

2.2 Characterization of Microstructure and Chemical Composition and Performance Tests

The thickness of coatings was measured using a stylus profilometer (AMBIOS XP-2, USA). The chemical composition of (Ti,Al)N coating was determined using an x-ray photoelectron spectrometer (XPS, XSAM800, UK), which was calibrated with the binding energy of C1*s* (284.6 eV) in graphite. An x-ray diffractometer (XRD, TD-3500, China) was used to evaluate the microstructure of the coatings using grazing incidence at an angle of 3° of the primary beam (Cu Kα radiation). The micro/nanohardness of the coatings was measured using a Vickers microhardness tester (TMVP-1, China) and nanoindenter (UMT-2, USA). The adhesion property of the coatings was evaluated by scratch tests (CSM scratch tester, Switzerland). The normal load of the indenter was linearly increased from 0 N to 100 N, and the scratch length was 5 mm. Wear tests (CSM tribometer, Switzerland) were performed to evaluate the tribological properties of the coatings. During the wear tests, Si_3N_4 balls (Φ 6 mm) were used as the friction partner; the normal load was 2 N; the sliding speed and laps were 2 cm/s and 6000 cycles, respectively. The wear tracks of the samples were observed using an optical microscope (Axio Image A1m, Germany) and a scanning electron microscope (SEM, Quanta 250, USA).

3. Results and Discussion

3.1 XPS Analyses of (Ti,Al)N Coatings

Figure 1 shows the XPS spectra of Al_{2p}, Ti_{2p}, and N_{1s} at different sputtering currents. The surface of all the (Ti,Al)N coatings were etched only 10 nm by Ar^+ before the XPS analyses. Therefore, O was clearly detected. As shown in Fig. 1(a), the intensity of Al_{2p} peaks increases with the sputtering current, indicating that the Al content in the coating gradually increased (Ref 21). This is probably because a strong sputtering current increases the sputtering rate of TiAl. The Ti evaporating deposition from the evaporation source is limited. The Al_{2p} peak of $(Ti,Al)_{5A}N$ can be split into two peaks at 73.4 and 74.2 eV. The peak at 73.4 eV can be attributed to the ternary compound (Ti,Al)N, indicating the formation of (Ti,Al)N coating (Ref 22). The higher binding energy (74.2 eV) component can be attributed to Al-O bond (Ref 23). The trend of XPS spectra of Ti_{2p} in Fig. 1(b) is consistent with Al_{2p}, i.e., the XPS profile of Ti_{2p} almost remained unchanged when the sputtering current was < 2.5 A. Four binding energy peaks were observed at 455.4, 457.6, 461, and 463.7 eV, corresponding to TiN, TiO*x*, TiO_2, and $Ti_{2p1/2}$, respectively. When the sputtering current was increased to 5 A, the XPS profile of Ti_{2p} clearly changed compared with other current values. One new binding energy peak located at 456.1 eV can also be attributed to TiN. Obviously, the binding energy of TiN increased by ∼ 0.7 eV; this may be caused by a high Al content (Ref 23). In the XPS spectra of N_{1s}, the binding energy of N (396.9 eV) shows a decreasing trend with the increase in sputtering current as shown in Fig. 1(c). This is because the binding energy of AlN is weaker than that of TiN (Ref 24). When the sputtering current reached up to 5 A, the central binding energy of the main peak decreased from 396.9 to 396.4 eV, indicating that TiN and AlN coexist in the coatings. Moreover, a binding energy peak of 398.2 eV was attributed to N-O bond.

To further obtain the composition of coatings with different sputtering currents, energy-dispersive x-ray spectroscopy (EDS) was carried out to analyze the elemental composition of coatings, and the results are shown in Table 2. As shown in Table 2, the Ti, Al, and N contents slightly changed when the sputtering current was increased from 0 A to 2.5 A. When the current was adjusted to 5 A, the Al and Ti contents increased from 1.0 to 31.8% and decreased from 58% to 29.6% compared with those of 2.5 A, respectively. The EDS results are consistent with the XPS results. Notably, the EDS detection depth was > 2 μm. Thus, O was undetected.

3.2 Structure of (Ti,Al)N Coatings

Figure 2 shows the XRD patterns of (Ti,Al)N coatings deposited with different sputtering currents. All the XRD patterns have similar profile, indicating a phase of cubic B1 NaCl-type (reference code: 03-065-0414) structure. Interestingly, the (111) lattice plane (∼ 36.5°) of (Ti,Al)N coatings showed strong diffraction peaks, but the (200) and (222) lattice planes of the coatings showed weaker diffraction peaks than that of (111) lattice plane. In addition, with the increase in sputtering current, Al was incorporated into the TiN coatings. A characteristic peak centered at 40.2° was observed and attributed to the hexagonal phase of Ti_2AlN (reference code: 03-065-3496). Another peak centered at 44.6° arose from an

Table 1 Deposition parameters and operating conditions of TiAlN coatings on HSS

Gas flow ratio	Pressure	Voltage	Deposition temperature	Sputtering current	Thickness
N_2:Ar = 4:1	0.5 Pa	− 150 V	270, 380, 420, 480 °C	0, 1.5, 2.5, 5 A	1.8 ± 0.2 μm

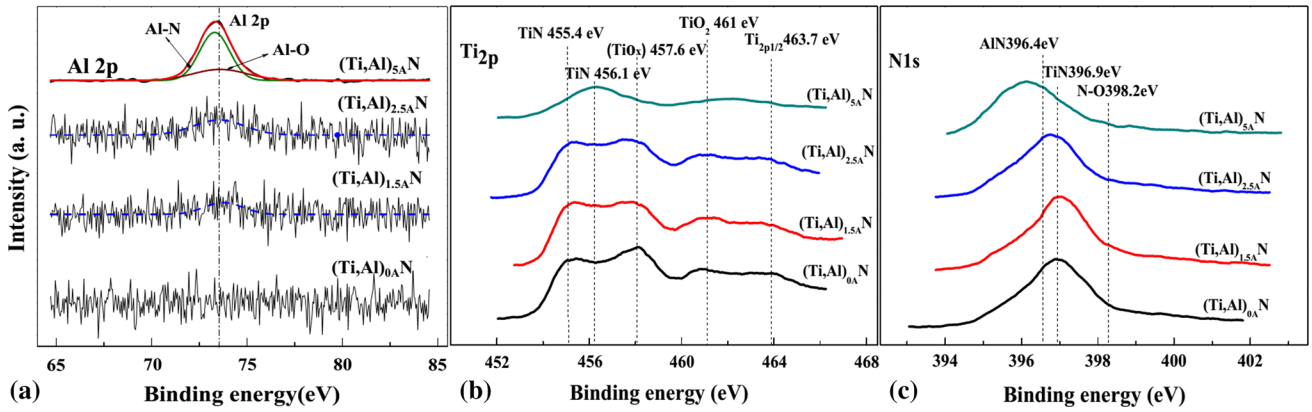

Fig. 1 XPS spectra of Al_{2p} (a), Ti_{2p} (b), N_{1s} (c) at different sputtering currents. The Al_{2p} peaks of $(Ti,Al)_{1.5A}N$, $(Ti,Al)_{2.5A}N$, and $(Ti,Al)_{5A}N$ were fitted by multipeaks Gaussian fitting

Table 2 Elemental contents of (Ti,Al)N coatings at different sputtering currents

	Composition (at.%)		
Samples	**Ti**	**Al**	**N**
$(Ti,Al)_{0A}N$	59.0	0.0	41.0
$(Ti,Al)_{1.5A}N$	58.5	0.2	41.2
$(Ti,Al)_{2.5A}N$	58.0	1.0	41.7
$(Ti,Al)_{5A}N$	29.5	31.8	38.6

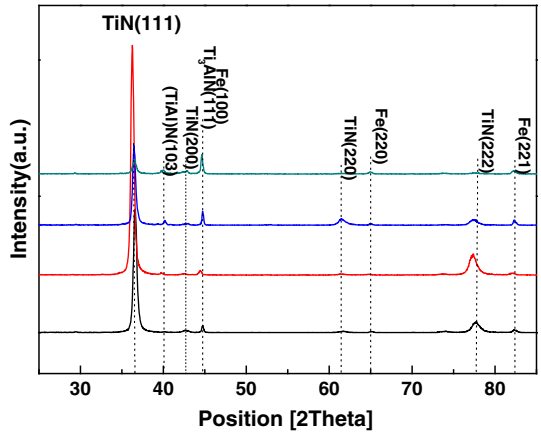

Fig. 2 X-ray diffraction (XRD) patterns of (Ti,Al)N coatings under the different fabrication condition

overlapping of peaks of Ti_3AlN (reference code: 03-037-1140) and Fe (reference code: 00-006-0696). When the sputtering current was > 2.5 A, the Al content increased rapidly, and the Ti_3AlN phase formed, increasing the peak strength. Meanwhile, the temperature of HSS increased due to the high-energy ion (Ar^+, N^+) sputtering of TiAl alloy. Therefore, the position of (111) diffraction peak showed a slight change in peak width and peak position; this can be ascribed to the variation in grain size. The position of (111) diffraction peak shifted from 36.5° to 36.1° with the increase in sputtering current (0-1.5 A), whereas the position of diffraction peak shifted back to 36.4° at 5 A. The position of (200) diffraction peak showed a similar change. The average grain sizes of the crystallites in (Ti,Al)N coatings can be calculated using the Scherrer equation (Ref 25).

$$d = \frac{k \times \lambda}{\beta \times \cos\theta} \quad \text{(Eq 1)}$$

where d, k, λ, β, and θ are the crystallite size, Scherrer constant, x-ray wavelength full width at half maximum (FWHM), and diffraction angle, respectively. Table 3 shows that the grain sizes of (Ti,Al)N coatings under different fabrication conditions are in the range of 0-2.5 A; the grain size of (Ti,Al)N coatings increased from 15.9 to 18.1 nm, indicating that a proper deposition temperature promotes the growth of TiN grains. When the sputtering current was increased to 5 A, the grain sizes of $(Ti,Al)_{5A}N$ rapidly decreased from 18.1 to 15.2 nm. In addition, the FWHM of (111) lattice plane also indicates that $(Ti,Al)_{2.5A}N$ has the maximum grain size. In general, the Al atoms hinder the growth of TiN grains, but temperature increase can promote the grain growth (Ref 26, 27). Therefore, the grain growth of (Ti,Al)N coatings is controlled by both Al content and deposition temperature. In other words, the effect of deposition temperature on grain growth is the main factor when the sputtering current was < 2.5 A. In contrast, the Al content became the main factor when the sputtering current was > 5 A. In this study, the maximum grain size of TiN was obtained at a sputtering current of 2.5 A.

3.3 Mechanical Properties

In this study, the average thickness of all the (Ti,Al)N coatings was determined as 1.8 ± 0.2 μm. This thickness was controlled by deposition time. Under relatively heavy applied load conditions (microhardness: 245 mN), the influencing area of indenter exceeds the thickness of coatings; therefore, the obtained hardness can be considered as the effective hardness

Table 3 Relative parameters of TiN(111) under different fabrication conditions

Parameters	$(Ti,Al)_{0A}N$	$(Ti,Al)_{1.5A}N$	$(Ti,Al)_{2.5A}N$	$(Ti,Al)_{5A}N$
2θ	36.5	36.1	36.8	36.4
FWHM	0.52	0.48	0.45	0.54
Grain sizes (nm)	15.9	17.2	18.1	15.2

Table 4 Microhardness/nanohardness and elastic modulus data of (Ti,Al)N coatings

Samples	HSS	$(Ti,Al)_{0A}N$	$(Ti,Al)_{1.5A}N$	$(Ti,Al)_{2.5A}N$	$(Ti,Al)_{5A}N$
Microhardness ($Hv_{0.025}$)	760 ± 54	1573 ± 90	2073 ± 71	1564 ± 65	1125 ± 62
Nanohardness (20 mN)	…	20 Gp	24 Gp	25 Gp	24 Gp
Elastic modulus	…	325 Gp	340 Gp	360 Gp	290 Gp

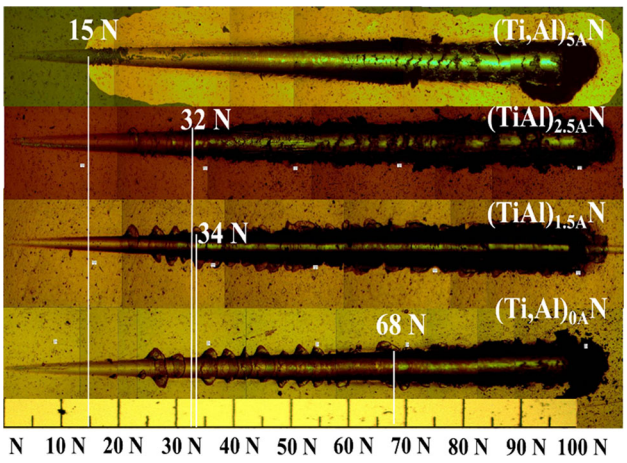

Fig. 3 Image of scratch tracks on the surface of (Ti,Al)N coatings

of the coating–substrate system (Ref 28). The results of micro/nanohardness tests and elastic modulus of all the (Ti,Al)N coatings with different sputtering currents are shown in Table 4. As shown in Table 4, the microhardness of bare HSS is only ~ 760 ± 54 HV, whereas the microhardness of the HSS substrate with a $(Ti,Al)_{0A}N$ coating was up to 1573 ± 90 HV. This indicates that $(Ti,Al)_{0A}N$ coating can effectively improve the hardness of the HSS substrate. Moreover, $(Ti,Al)_{1.5A}N$ substrate showed a significant increase in microhardness (2073 ± 71 HV). This is probably because some Ti atoms in TiN lattice were replaced with Al atoms, and the radius of Al atom (0.143 nm) is shorter than that of Ti atom (0.146 nm). This leads to lattice distortion and an increase in the dislocation density. These changes can improve the hardness of the coating (Ref 24). In addition, the XPS data (Fig. 1) show that high-hardness AlN and TiN phases coexist in the (Ti,Al)N coatings. However, the microhardness of composite coating significantly decreased when using a sputtering current of > 1.5 A. A high sputtering current increases the cavity temperature, leading to the softening of HSS substrate (Ref 29). Therefore, the microhardness of coating–substrate system decreased. To further obtain the information about coatings, the nanohardness and elastic modulus of (Ti,Al)N coatings were measured using an indentation tester. During the nanohardness testing, the total hardness consists of the hardness of coating and HSS substrate because of an indentation depth of 1.1 μm (Ref 28, 30). Table 4 shows that both the maximum nanohardness and elastic modulus of the (Ti,Al)N coating were 25 GPa and 360 GPa, respectively, when the sputtering current was set at 2.5 A.

3.4 Adhesion of (Ti,Al)N Coatings

The adhesion property of (Ti,Al)N coatings was evaluated by scratch tests, and the normal load of indenter was linearly increased from 0 to 100 N. With the increase in normal load, the substrate reached a critical deformation, and the (Ti,Al)N coatings detached from the HSS substrate at different scratch forces. Figure 3 shows the image of scratch tracks of (Ti,Al)N coatings on HSS. A range of failure events occurred along the length of the scratch track, and the degree of damaged coatings such as spallation and buckling depends on the adhesion of coatings. To evaluate the adhesion of coatings, a minimum critical load that detaches the coatings from the HSS substrate with full exposure of the substrate should be determined. $(Ti,Al)_{0A}N$ coating showed edge cracking at a load of 25 N, and a large-area chipping occurred at 68 N with the exposure of the substrate. With the increase in sputtering current, the critical load gradually decreased from 68, 34, and 32-15 N. The differences in the scratching response for different (Ti,Al)N coatings are clearly shown. This result indicates that the increase in sputtering current decreases the adhesion. The scratch tracks in $(Ti,Al)_{0A}N$, $(Ti,Al)_{1.5A}N$, and $(Ti,Al)_{2.5A}N$ coatings showed tensile arc cracks; the failure was mainly due to the cracking and fragmentation of the coating when the indenter was depressed on the coating–substrate system. $(TiAl)_{5A}N$ coating showed a large chipping at 15 N; the worse critical load behavior of $(TiAl)_{5A}N$ coating compared with other samples at a lower puttering current can be attributed to the softening of substrate during the high-temperature deposition. Considering the same applied load during the scratch testing, the plastic deformation of the substrate should be much higher in the softened substrate because of its low yield strength. The coating is subjected to a higher strain, increasing the cracking probability. This distributes these fragments of coating along the two sides of scratch. In other words, a high sputtering current not only increases the Al content in coating, but also softens the HSS substrate. These results indicate the important parameters (sputtering current, Al content, and deposition temperature) for the collapse of coatings (Ref 31).

3.5 Wear Property and Antiwear Mechanism of (Ti,Al)N Coating

The wear resistance of (Ti,Al)N coatings was tested using a dry ball-on-disk device. Figure 4 shows the friction coefficient of all the (Ti,Al)N coatings with laps. As shown in Fig. 4, $(Ti,Al)_{1.5A}N$ coating had a minimum friction coefficient of 0.54 in the wear stable zone, whereas $(Ti,Al)_{2.5A}N$ coating had an average friction coefficient of 0.74. This is caused by a higher hardness, making velocity accommodation in the sliding contact more difficult (Ref 32). Unusually, the friction coefficient of $(Ti,Al)_{5A}N$ coating showed a very strong vibration throughout the testing. Finally, a value of 0.63 was obtained; this value is close to the friction coefficient of $(Ti,Al)_{0A}N$ coating (0.61). This is probably because poor cohesion causes the peeling of $(Ti,Al)_{5A}N$ coating from TiN interlayer during the friction force test, i.e., the actual wear test occurs between the TiN coating and Si_3N_4 spheres. Therefore, the friction coefficients of $(Ti,Al)_{5A}N$ and $(Ti,Al)_{0A}N$ coatings are almost similar.

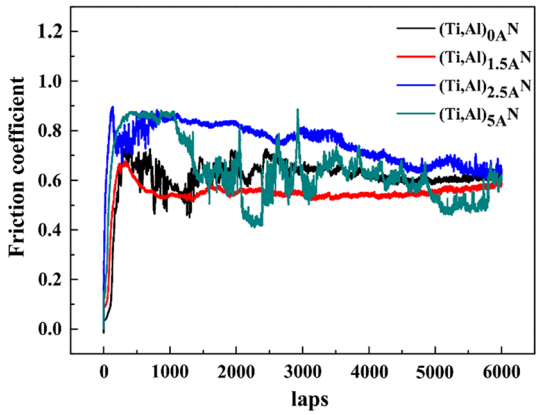

Fig. 4 Friction coefficient of (Ti,Al)N coatings

Figure 5(a), (b), (c), (d), and (e) shows the wear trace on the surface of HSS substrate, (Ti,Al)N coatings, and Si_3N_4 balls; with a sliding distance of 107 m. As shown in Fig. 5(a), typical deep and wide wear furrows and a clear groove full of black debris were observed on the HSS substrate; the wear track had a maximum depth of 1.5 μm and width of 560 μm. Interestingly, the wear track depth and width of all the (Ti,Al)N coatings showed a relatively low value compared with those of HSS substrate. In particular, $(Ti,Al)_{2.5A}N$ had a minimum depth value of 0.3 μm, indicating that $(Ti,Al)_{2.5A}N$ coatings have a higher wear resistance. Notably, the wear resistance decreased when the sputtering current was set at 5 A, which softens the HSS substrate at a high temperature. Therefore, the adhesion of $(Ti,Al)_{5A}N$ coating was weaker than that of $(Ti,Al)_{2.5A}N$ coating, leading to a relatively weaker wear property.

To further analyze the antiwear mechanism of (Ti,Al)N coatings, three coatings, $(Ti,Al)_{0A}N$, $(Ti,Al)_{2.5A}N$, and $(Ti,Al)_{5A}N$ were investigated using SEM and EDS. The morphology of wear tracks and EDS spectra of (Ti,Al)N coatings are shown in Fig. 6 and 7, respectively. The EDS spectra (Fig. 7) show the presence of O in the wear tracks of these three coatings, indicating that oxidation occurred during the test. The main morphologies of $(Ti,Al)_{0A}N$ and $(Ti,Al)_{2.5A}N$ coatings are shown in Fig. 6(a) and (b), respectively. The accumulated debris was distributed along the edge of wear tracks. This

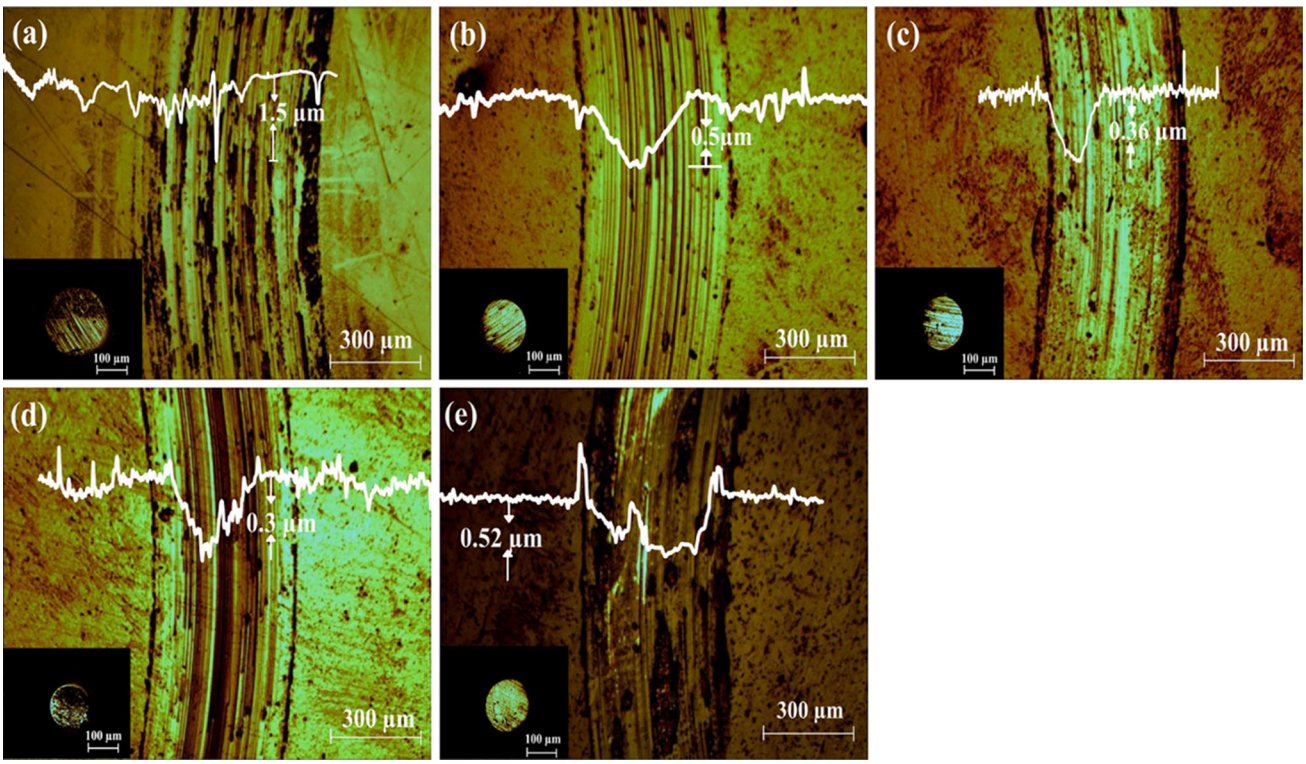

Fig. 5 Wear traces of HSS substrate with TiN and (Ti,Al)N coatings. (a) HSS substrate, (b) $(Ti,Al)_{0A}N$, (c) $(Ti,Al)_{1.5A}N$, (d) $(Ti,Al)_{2.5A}N$, and (e) $(Ti,Al)_{5A}N$. The white contour line in each image represents line-scan; the pictures of lower-left quarter zone show Si_3N_4

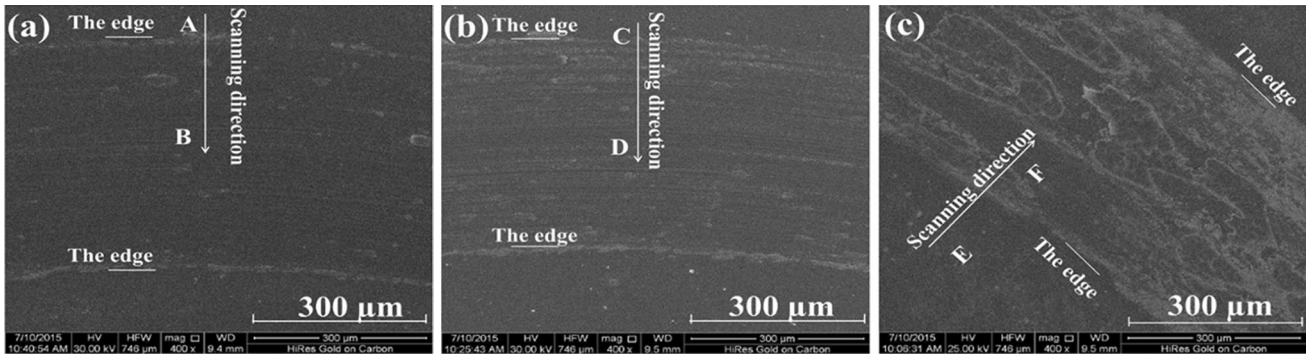

Fig. 6 SEM images of wear tracks. (a) $(Ti,Al)_{0A}N$, (b) $(Ti,Al)_{2.5A}N$, and (c) $(Ti,Al)_{5A}N$

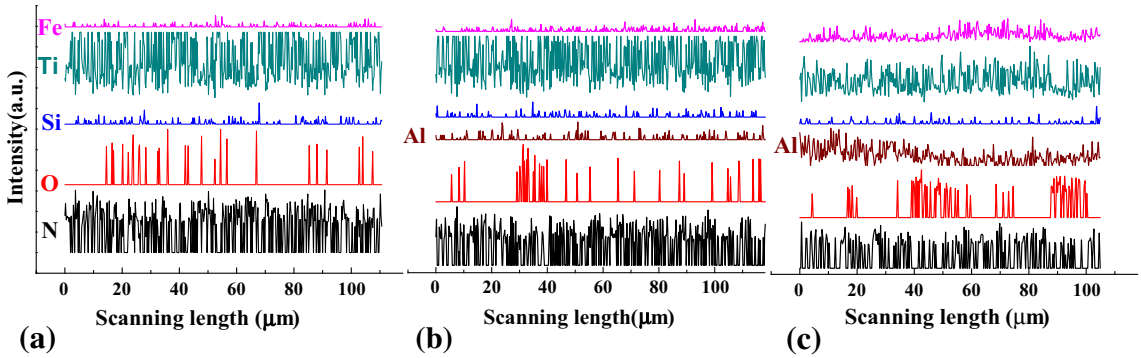

Fig. 7 EDS spectra of wear tracks. (a) $(Ti,Al)_{0A}N$, (b) $(Ti,Al)_{2.5A}N$, and (c) $(Ti,Al)_{5A}N$

phenomenon shows that the debris can be easily ejected from the friction zone. Regarding the wear mechanism, the SEM image of $(Ti,Al)_{0A}N$ coating shows an uneven surface and micro-islands in the center of the track related to the continuous and repetitive plastic flow of coating and debris. Along the EDS scanning direction from the edge (zone A) to the center of the wear track (zone B), the elemental composition shows a slight variation from the bulk to the wear track center. This result shows that $(Ti,Al)_{0A}N$ coating is not damaged. The main wear mechanism can be explained by abrasive wear for $(Ti,Al)_{0A}N$ coating. In addition, for $(Ti,Al)_{2.5A}N$ coating, many paratactic scratch grooves along the sliding direction were observed on the wear track surface; they can be attributed to the brittle fracture of the coating itself. The fractured hard coating and the debris from the ball on track acted as scratch indenters under the action of vertical acting load, forming the grooves. Herein, the wear mechanism can be explained by the abrasive wear and oxidation of $(Ti,Al)_{2.5A}N$ coating.

Figure 6(c) and 7(c) show the SEM image and EDS spectra of $(Ti,Al)_{5A}N$ coating, respectively. The SEM image shows that the coating is worn by plowing and mechanical domination wear. This type of damage is not caused by a gradual wear process, but it is caused via a brittle failure mechanism. Along the wear trace direction, severe irregularity was formed in the friction zone. In other words, some zones had incomplete coating, but other zones lost the coating completely. Brittle failure mechanism may play the role of a third body in the tribological system. Along the EDS scanning direction from the edge (zone E) to the center of the wear track (zone F), the Al content decreased, but the O signal suddenly increased at the edge of wear track. This result shows that $(Ti,Al)_{5A}N$ coating is partially damaged. The mechanism of $(Ti,Al)_{5A}N$ coating consists of a mixture of abrasive wear, oxidation, adhesive wear, and brittle failure (Ref 33).

4. Conclusions

(Ti,Al)N coatings were deposited on HSS substrates by combined plasma-enhanced magnetron sputtering and ion-plating evaporation technique. The effects of sputtering current on microstructure and properties were investigated. Multiple characterization and testing techniques were used to establish the structure–property relationship of (Ti,Al)N coatings. XPS characterization indicated that the coating consisted of a mixture of TiN and AlN when the sputtering current was 5 A. However, the main composition was TiN when the sputtering current was $<$ 2.5 A. The XRD data indicated that both the grain size and growth of (Ti,Al)N coatings were affected by sputtering current. The effects of structure on the properties of (Ti,Al)N coatings such as hardness, adhesion, and tribological and antiwear properties were investigated. The results show that a suitable sputtering current was beneficial to improve the performance of (Ti,Al)N coatings on HSS substrates. In addition, the HSS substrate could be softened at a high sputtering current, leading to poor hardness and antiwear properties. Hence, the optimal value of sputtering current for

the deposition of (Ti,Al)N coating was determined as 2.5 A using our technique.

Acknowledgments

This work was financially supported by the Basic and Frontier Research Program of Chongqing Municipality (cstc2016jcyjA0451), Scientific and Technological Research Program of Chongqing Municipal Education Commission (KJ1601104), The Foundation of Chongqing University of Art and Sciences (Y2015XC24, 2017RXC25), Natural Science Foundation of China (21603020), and NSAF (51275323).

References

1. J. Wang, Y.B. Liu, J. An, and L.M. Wang, Wear Mechanism Map of Uncoated HSS Tools During Drilling Die-Cast Magnesium Alloy, *Wear*, 2008, **265**, p 685–691
2. V. Braic, C.N. Zoita, M. Balaceanu, A. Kiss, A. Vladescu, A. Popescu, and M. Braic, TiAlN/TiAlZrN Multilayered Hard Coatings for Enhanced Performance of HSS Drilling Tools, *Surf. Coat. Technol.*, 2010, **204**, p 1925–19288
3. R. Venkatesh, V.S. Rao, N. Arunkumar, S. Biswas, and R.S. Kumar, Wear Analysis on Silicon Carbide Coated HSS Pin on SS Disc Substrate, *Proc. Mater. Sci.*, 2015, **10**, p 644–650
4. W.W. Wu, W.L. Chen, S.B. Yang, Y. Lin, S.H. Zhang, and T.Y. Cho, Design of AlCrSiN Multilayers and Nanocomposite Coating for HSS Cutting Tools, *Appl. Surf. Sci.*, 2015, **351**, p 803–810
5. Z. Zheng and Z. Yu, Characteristics and Machining Applications of Ti(Y)N Coatings, *Surf. Coat. Technol.*, 2010, **204**, p 4107–4113
6. L. Chen, M. Moser, Y. Du, and P.H. Mayrhofer, Compositional and Structural Evolution of Sputtered Ti-Al-N, *Thin Solid Films*, 2009, **517**, p 6635–6641
7. A. Rizzo, L. Mirenghi, M. Massaro, U. Galietti, L. Capodieci, R. Terzi, L. Tapfer, and D. Valerini, Improved Properties of TiAlN Coatings Through the Multilayer Structure, *Surf. Coat. Technol.*, 2013, **235**, p 475–483
8. L. Chen, K.K. Chang, Y. Du, J.R. Li, and M.J. Wu, A Comparative Research on Magnetron Sputtering and Arc Evaporation Deposition of Ti-Al-N Coatings, *Thin Solid Films*, 2011, **519**, p 3762–3767
9. J.Y. Yan, D.J. Li, L. Dong, C.K. Gao, N. Wang, X.Y. Deng, H.Q. Gu, R.X. Wan, and X. Sun, The Modulation Structure Induced Changes in Mechanical Properties of TiAlN/Al_2O_3 Multilayers, *Nucl. Instrum. Methods Phys. Res. Sect. B*, 2013, **307**, p 123–126
10. H. Du, H. Zhao, and J.G. Xian, Effect of Interlayers on the Structure and Properties of TiAlN Based Coatings on WC-Co Cemented Carbide Substrate, *Int. J. Refract. Metals Hard Mater.*, 2013, **37**, p 60–66
11. L. Tomaszewski, W. Gulbinski, A. Urbanowicz, T. Suszko, A. Lewandowski, and W. Gulbinski, TiAlN Based Wear Resistant Coatings Modified by Molybdenum Addition, *Vacuum*, 2015, **121**, p 223–229
12. L.H. Zhu, M.M. Hu, W.Y. Ni, and Y.X. Liu, Effect of Al Content on Adhesion Strength of TiAlN Coatings, *Vacuum*, 2012, **12**, p 1795–1799
13. M.A. Al-Bukhaiti, K.A. Al-hatab, W. Tillmann, F. Hoffmann, and T. Sprute, Tribological and Mechanical Properties of Ti/TiAlN/TiAlCN Nanoscale Multilayer PVD Coatings Deposited on AISI, H11 Hot Work Tool Steel, *Appl. Surf. Sci.*, 2014, **318**, p 180–190
14. T. Mori, M. Noborisaka, T. Watanabe, and T. Suzuki, Oxidation Resistance and Hardness of TiAlSiN/CrAlYN Multilayer Films Deposited by the Arc Ion Plating Method, *Surf. Coat. Technol.*, 2012, **213**, p 216–220
15. A. Inspektor and P.A. Salvador, Architecture of PVD Coatings for Metalcutting Applications: A Review, *Surf. Coat. Technol.*, 2014, **257**, p 138–153
16. G.S. Fox-Rabinovich, B.D. Beake, J.L. Endrino, S.C. Veldhuis, R. Parkinson, L.S. Shuster, and M.S. Migranov, Effect of Mechanical Properties Measured at Room and Elevated Temperatures on the Wear Resistance of Cutting Tools with TiAlN and AlCrN Coatings, *Surf. Coat. Technol.*, 2006, **200**, p 5738–5742
17. P. Panjan, B. NavinŠek, M. Čekada, and A. Zalarb, Oxidation Behaviour of TiAlN Coatings Sputtered at Low Temperature, *Vacuum*, 1999, **53**, p 127–131
18. A. Obrosov, R. Gulyaev, M. Ratzke, A.A. Volinsky, S. Bolz, M. Naveed, and S. Wei, XPS and AFM Investigations of Ti-Al-N Coatings Fabricated Using DC Magnetron Sputtering at Various Nitrogen Flow Rates and Deposition Temperatures, *Metals*, 2017, **7**, p 1–10
19. S. Sveen, J.M. Andersson, R.M. Saoubi, and M. Olsson, Scratch Adhesion Characteristics of PVD TiAlN Deposited on High speed Steel, Cemented Carbide and PCBN Substrates, *Wear*, 2013, **308**, p 133–141
20. Y.Y. Su, J.B. Wang, L.L. Tian, H.B. Zhao, M.J. Tu, and L.J. Zhao, Effect of Al Doped on Microstructure and Properties of TiN Coating, *Funct. Mater.*, 2013, **44**, p 2668–2671
21. K. Kutschej, P.H. Mayrhofer, M. Kathrein, P. Polcik, R. Tessadri, and C. Mitterer, Structure, Mechanical and Tribological Properties of Sputtered $Ti_{1-x}Al_xN$ Coatings with 0.5 V $\leq$ x $\leq$ 0.75V, *Surf. Coat. Technol.*, 2005, **200**, p 2358–2365
22. J.C. Oliveira, A. Manaia, and A. Cavaleiro, Hard Amorphous Ti-Al-N Coatings Deposited by Sputtering, *Thin Solid Films*, 2008, **516**, p 5032–5038
23. D.H. Jung, K. Moon, S.Y. Shin, and C.S. Lee, Influence of Ternary Elements (X = Si, B, Cr) on TiAlN Coating Deposited by Magnetron Sputtering Process with Single Alloying Targets, *Thin Solid Films*, 2013, **546**, p 242–245
24. N. Jiang, Y.G. Shen, H.J. Zhang, S.N. Bao, and X.Y. Hou, Superhard Nanocomposite Ti-Al-Si-N Films Deposited by Reactive Unbalanced Magnetron Sputtering, *Mater. Sci. Eng. B*, 2006, **135**, p 1–9
25. V. Uvarov and I. Popov, Metrological Characterization of X-ray Diffraction Methods for Determination of Crystallite Size in Nano-scale Materials, *Mater. Charact.*, 2007, **58**, p 883–891
26. S.P. Pemmasani, K. Valleti, and C. Gundakaram, Effect of Microstructure and Phase Constitution on Mechanical Properties of $Ti_{1-x}Al_xN$ Coatings, *Appl. Surf. Sci.*, 2014, **313**, p 936–946
27. C. Wang, S. Ou, and S.Y. Chiou, Microstructures of TiN, TiAlN and TiAlVN Coatings on AISI, M2 Steel Deposited by Magnetron Reactive Sputtering, *Trans. Nonferrous Metals Soc. China*, 2014, **24**, p 2559–2565
28. J.Y. Yan, Y.D. Sun, D.J. Li, M.Y. Liu, L. Dong, M. Cao, and C.K. Gao, High-Temperature Stability of TiAlN/TiB_2 Multilayers Grown on Al_2O_3 Substrates Using IBAD, *Surf. Coat. Technol.*, 2013, **229**, p 105–108
29. W.Z. Li, H.W. Liu, M. Evaristo, T. Polcar, and A. Cavaleiro, Influence of Al Content on the Mechanical Properties and Thermal Stability in Protective and Oxidation Atmospheres of Zr-Cr-Al-N Coatings, *Surf. Coat. Technol.*, 2013, **236**, p 239–245
30. Y.Y. Su, X. Gui, D. Xie, and S.Y. Li, The Effect of a TiN Interlayer on the Tribological Properties of Diamond-Like Carbon Films Deposited on 7A04 Aluminum Alloy, *IEEE Trans. Plamsa Sci.*, 2011, **39**, p 3144–3148
31. P. Li, L. Chen, S.Q. Wang, B. Yang, Y. Du, J. Li, and M.J. Wu, Microstructure, Mechanical and Thermal Properties of TiAlN/CrAlN Multilayer Coatings, *Int. J. Refract. Metals Hard Mater.*, 2013, **40**, p 51–57
32. B. Grossmann, N. Schalk, C. Czettl, M. Pohler, and C. Mitterer, Phase Composition and Thermal Stability of Arc Evaporated $Ti_{1-x}Al_xN$ Hard Coatings with 0.4 $\leq$ x $\leq$ 0.67, *Surf. Coat. Technol.*, 2017, **309**, p 687–693
33. C.L. Liang, G.A. Cheng, R.T. Zheng, and H.P. Liu, Fabrication and Performance of TiN/TiAlN Nanometer Modulated Coatings, *Thin Solid Films*, 2011, **520**, p 813–817